Proceedings of ASME Turbo Expo 2023
Turbomachinery Technical Conference and Exposition
GT2023
June 26-30, 2023, Boston, Massachusetts, USA

GT2023-103205

Hydrogen-Enriched Natural Gas Co-Firing: A Comparison of FGM and EDC Models

Rang Zhao **Uyioghosa Igie** **David Abbott**

Centre for Propulsion and Thermal Power Engineering,
Cranfield University
Cranfield, Bedfordshire, MK43 0AL, England

ABSTRACT

To facilitate the transition from natural gas to a future hydrogen economy, the combustion of natural gas/hydrogen blends in gas turbines will play an important role in power generation. The influence of hydrogen content on technically premixed swirl-stabilized flame using large eddy simulation has proven to be powerful but with high computational costs. Hence, RANS-based models are useful for preliminary investigations and sensitivity studies. Flamelet Generated Manifold (FGM) and Eddy-Dissipation Concept (EDC) are two widely used RANS-based combustion models. EDC, in particular, accounts for the interaction between chemistry and turbulence using detailed chemical mechanisms, but at the cost of higher computational resources. FGM preprocesses the flamelet as a function of mixture fraction and progress variable and pre-integrates the chemistry-turbulence interaction into a Probability Density Functions (PDF) table, which makes FGM computationally inexpensive. This study aims to compare the predictions of these models with experimental data of a methane-fueled technically premixed swirl-stabilized low-pressure burner. The better-performing model is used to evaluate the influence of methane and hydrogen blends (up 40% by volume) in a higher-pressure burner also validated with experiments. The study has shown that EDC produces better agreement with the experimental data than FGM in estimating the flame temperature, flow velocity, and carbon dioxide profiles. FGM did not correctly capture the flame pattern and overestimated the reaction rate. This is possibly due to its simplified preprocessed chemistry mechanism, which could not evaluate the local thermal properties of the gas mixture properly. For the higher pressure evaluation at 5 bar, the EDC model captured the influence of hydrogen content addition on flame behaviour. As the hydrogen content increased, the chemical reaction rate increased, and the flame length indicated by OH decreased. This reduction in flame length is consistent with the experimental results. The CFD showed that at 20% H_2, the change in NOx emission compared to 100% methane is negligible using the mass of NO_X per unit of heat release calculation. A slight increase in NOx is shown for the same case using the concentration by volume corrected to 15% O_2 approach. Nevertheless, both approaches showed NOx reductions at 40% H_2. This study has shown that the behaviour of a technically premixed swirl-stabilized flame-firing methane/hydrogen blend is well represented by a non-adiabatic RANS-EDC model with low computation cost. This confirms its applicability in evaluating acceptable lean premixed burners characteristics for gas turbines.

Keywords: FGM, EDC, hydrogen, methane, radiation, discrete ordinates, WSGG

Nomenclature

EDC	Eddy dissipation concept
FGM	Flamelet-generated manifold
LHV	Lower heating value
ε	Emissivity
α	Absorptivity
Nu	Nusselt number
h	Convection coefficient
ISL	Inner shear layer
OSL	Outer shear layer
P_{th}	Fuel energy input [kW]
p_{comb}	Combustor chamber mean pressure
IRZ	Inner recirculation zone
ORZ	Outer recirculation zone
PIV	Particle image velocimetry
OH*-PLIF	OH* Planar laser-induced fluorescence
OH*-CL	OH* Chemiluminescence

1. INTRODUCTION

The combustion of hydrogen (H_2) is challenging for existing natural gas-fuelled gas turbines, because H_2 has higher reactivity than methane (CH_4), resulting in higher flame speed and greater flashback risk[1]-[4]. To facilitate the transition from natural gas to a future hydrogen economy, the combustion of CH_4/H_2 blends using existing combustor designs will play an important role in electric power generation.

High-resolution LES is a powerful CFD tool to model flame characteristics, but the computation time and cost are too high for preliminary investigations. These investigations could be enhanced by a reliable RANS-based approach which can capture the major characteristics of hydrogen-enriched natural gas flame with inexpensive computation time and cost.

Flamelet-generated manifold (FGM) and eddy dissipation concept (EDC) approaches are two RANS combustion models

widely applied in CFD works [5]-[6]. Shrivastava et al. [7] compared the performance of FGM and the EDC in modelling CH_4/H_2 flame with three configurations: jet flame, bluff-body stabilized flame and micromix flame. That study showed that both FGM and EDC could produce reasonable predictions, but EDC is relatively computationally expensive. Zghal et al. [6] applied the FGM and EDC to model a hydrogen-fueled micro-mix burner and concluded that both FGM and EDC can capture the features of micro-mix flame well. Patil et al. [8] compared the performance of EDC and FGM in evaluating a CH_4-fuelled single-jet flame near lean blowout conditions; the study confirmed that EDC yielded closer agreement with measured results than FGM in capturing lean flame behaviours, as shown in **Figure 1**. This figure shows that with increasing centerline distance away from the jet flame, the FGM model generally poorly predicts the temperature profiles, compared to the EDC.

Nevertheless, previous studies in the open literature have not compared the performance of FGM and EDC on CH_4 in a technically premixed swirl-stabilized flame. This is an important research gap given that most practical burners are technically premixed; hence, the focus of this study

.

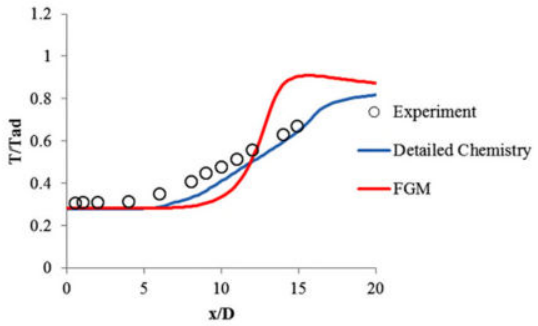

Figure 1. Single jet flame centerline temperature profiles: experiment, FGM and Detailed Chemistry (EDC)[8]

The flowchart presented in **Figure 2** shows the approach to the investigation. This study used RANS-FGM and RANS-EDC to model a CH_4 technically premixed swirl-stabilized flame at atmospheric pressure conditions and compared the CFD results with corresponding experimental data. The geometry of the low-pressure PRECCINSTA burner was provided with the support of the German Aerospace Center (DLR). Also, the experimental data for the validation was provided by DLR, and published in Refs [9]-[10]. The first part of the study includes a comparison of the FGM and EDC models, accounting for the heat loss of conduction, convection and radiation. The second part of the study considers the better of the two models at higher pressure (5 bar) conditions with CH_4/H_2 blends (0 to 40 vol% H_2). This analysis was evaluated using the DLR high-pressure PRECCINSTA burner geometry and experimental data [11]. The experimental data is used to verify the reliability of this CFD model in capturing the impact of added H_2 content on the flame shape and reaction rate. Also, the impact on NO_X production with fixed fuel energy input is investigated in the numerical model.

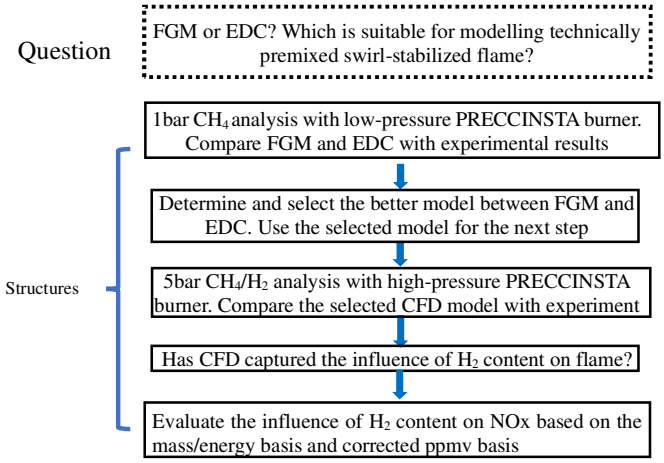

Figure 2. Flow chart of work structure

2. BURNER MODELS UNDER INVESTIGATION AND GRID INDEPENDENCE

2.1 Low and Higher Pressure Burner Configurations

This section introduces the two PRECCINSTA burners: the CH_4-fueled low-pressure case, and the CH_4/H_2 -fueled higher pressure burner shown in **Figure 3** and **Figure 4,** respectively. The low-pressure burner can produce a swirl-stabilized flame, and it has been numerically and experimentally studied under atmospheric conditions [9][12]-[14]. It comprises an upstream air plenum, a technical premix swirler, and a downstream rectangular chamber of 85mm by 85mm by 114mm with inert chamber walls. Inside the swirler, there are 12 fuel tubes injecting fuel into the crossflow fresh air (in a jet in crossflow configuration). The high-pressure PRECCINSTA burner has a similar swirler structure and a longer chamber of 80mm by 80mm by 200mm. A noticeable difference is the high-pressure burner has two cooling channels. This is for the bulkhead and chamber outer wall separately (i.e., cooling flow E and flow F in **Figure 4**). This study only accounts for the bulkhead cooling system (flow E), because flow F is not channeled into the combustion zone. Rather, the cooling effect of flow F is represented by an estimated external forced convection coefficient (h) that is an input to the CFD model. Details of the heat transfer model are provided subsequently.

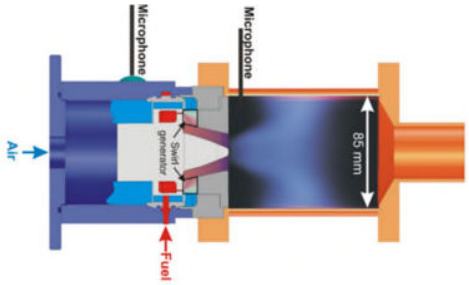

Figure 3. Schematic of low-pressure PRECCINESTA burner [9]

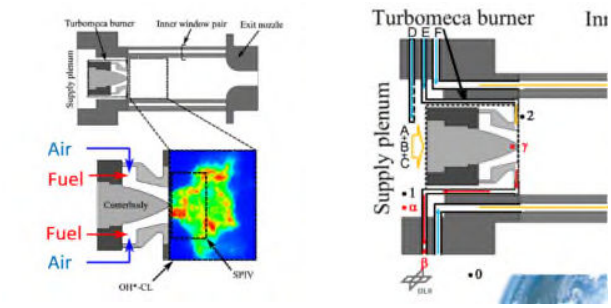

Figure 4. Schematic of higher-pressure PRECCINSTA burner [15]

Figure 5 shows the expected general flow pattern of this type of swirl-stabilized flame, where the swirler creates a swirling flow. The inner recirculation zone (IRZ) is sustained by the adverse pressure gradient due to centrifugal swirling flow, and a bluff body that is usually located at the centre. This is to prevent the reverse flow from penetrating upstream back to the mixing tube. The outer recirculation zone (ORZ) is sustained by the swirling flow and confined by the chamber walls. The fresh gas in-flow is located between the inner shear layer (ISL) and the outer shear layer (OSL). Subsequent analysis of the burners showcases the area zones that ensure that the flame is adequately anchored.

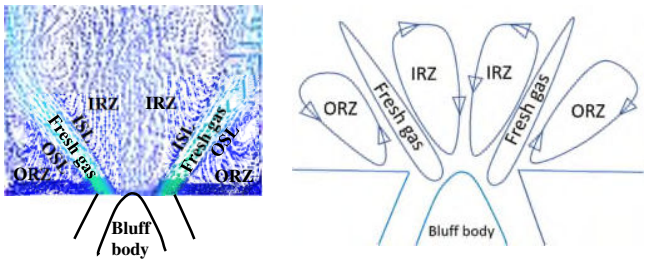

Figure 5. Schematic of swirl-stabilized flame

2.2 Grid Independence Study

The computational mesh for the 3D geometries was generated in ICEM-CFD 2021R1. Given the geometry of the model, the domain was discretized using both tetrahedral meshes in the burner section, and hexahedral meshes for the chamber. Also, a y+ of around 30 was used in combination with an enhanced wall function that is insensitive to the y+. **Figures 6** and **7** show the hybrid meshes for both burners, respectively. As the geometry of them are similar, this work only performed a full grid independence study for the higher pressure burner at 5 bar with CH_4 as fuel. Three grid cases were considered with a total of 4, 6 and 9 million nodes. The computation time of the 4 million and 9 million nodes is roughly 0.6 and 1.5 times that of the 6 million. **Figure A1** of **Appendix A** shows that the 6 million node case produced good accuracy in terms of temperature, CO_2, and axial velocity, with no significant improvement when using the finer mesh. Therefore, both burners were modelled with their corresponding 6 million grid.

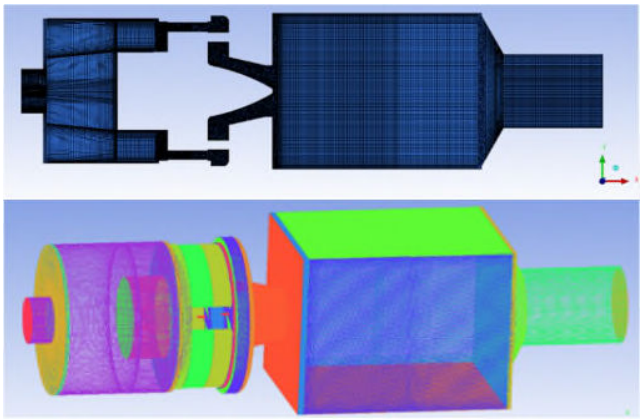

Figure 6. Grid for low-pressure burner

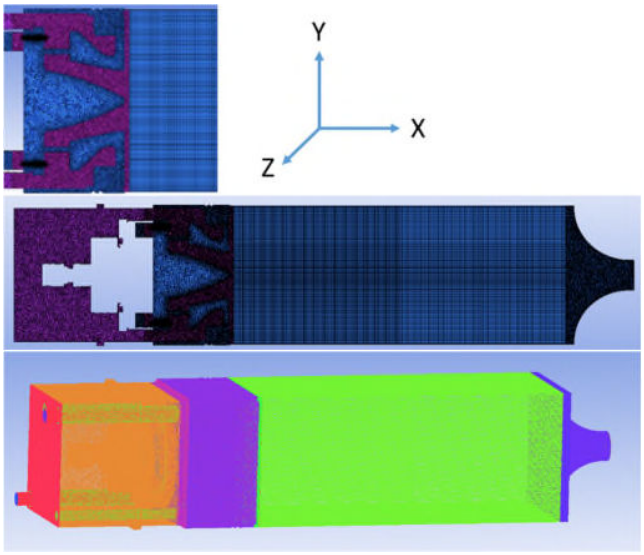

Figure 7. Grid for higher pressure burner

3. NUMERICAL METHODOLOGY

3.1 Turbulence and Combustion Models

The Realizable k-ε (RKE) and standard k-**Ω** are two popular turbulence models available in Ansys Fluent 2021R1 [16] used. Realizable k-ε is good at simulating the away-wall bulk flow and swirling flow, while standard k-**Ω** has a better performance in evaluating near-wall boundary layers[16]. Both models were compared as shown in **Figure B1** of **Appendix B** which is based on the low pressure case at 1 bar, with pure CH_4. These are both compared to the experimental data [9]. The RKE produces better agreement with experimental data than standard k-**Ω**, therefore, the former was adopted in this work.

The combustion models considered are the Flamelet-generated manifold (FGM) and eddy dissipation concept (EDC). These are two widely used combustion models[5]-[6]. FGM assumes the 3-D flame as an ensemble of several 1-D laminar flames[17] and can account for detailed 1-D flame chemistry and the effects of convection and diffusion. In the FGM system, the flamelets are pre-processed by describing the thermochemical trajectories as a function of mixture fraction and progress

variable (known as flamelet tables). The turbulence-chemistry interaction is also pre-integrated into a table of Probability Density Functions (PDF) by FGM, where the reaction process is represented by scalar mean value and scalar variance[18]. Therefore, the FGM is featured by pre-processing detailed chemistry. This makes FGM relatively computationally inexpensive.

However, FGM also has some limitations. Sun et al. [19] and Shrivastava et al. [7] identified that FGM assumes the Lewis number is unity, which is a reasonable assumption for pure CH_4 but not necessarily appropriate for CH_4/H_2 blends, where CH_4 has an approximate unity Lewis number and it gradually decreases to 0.6 as H_2 is blended [20]. Another shortcoming identified by Sun et al. [19] and Shrivastava et al. [7] was that FGM assumes a single constant turbulent Schmidt number Sc_t for the whole flow region, however the local turbulent Schmidt number should be determined by local turbulence[21]-[22].

EDC is an extension of the Eddy breakup model and assumes that reactions occur on small turbulent structures (named "fine-scale"). It can take detailed chemistry reactions into turbulence simulation and needs to solve transport equations for each species, rather than pre-process the chemistry as in FGM. This makes EDC relatively computationally expensive[8][23]. Jella et al.[24] applied EDC to model SGT-100 (a lean-premixed swirl-stabilized combustor) in both RANS and LES approaches, and showed EDC was more suitable for LES rather than RANS because the chemical reaction rate was related to instantaneous thermodynamic fluctuations.

The GRI-mech3.0 [25] is a chemistry kinetic mechanism widely used to model natural gas flames. Its use in CFD is proposed by several works including Refs[8][10][26]. When modelling the co-firing of CH_4/H_2 blends, it is generally recommended to use the GRI-3.0 chemical kinetic mechanism for low hydrogen concentrations (<50%). For higher hydrogen blends, alternative mechanisms such as San Diego, O'Conaire, and Aramco 1.3 [27] are typically suggested [4][27]. However, Aramco 1.3 contains a much larger number of species and reaction equations (316 species and 1805 reactions) [27] compared to GRI-3.0 (53 species and 325 reactions). As a result, Aramco 1.3 substantially increases the computational time required to solve the transport equations for each species using the EDC model. To strike a balance between computational efficiency and accuracy, this study used GRI-3.0 to model up to 40% H_2, despite limitations associated with its kinetic description [28].

3.2 Radiation Model (DO and WSGG Model)

To adequately simulate the operating conditions of the rig, it is necessary to incorporate the effects of radiation, convection, and conductive heat losses in the modelling process. In **Figures 8** and **9**, the surface radiative heat loss was determined by the chamber wall material and the gaseous radiation was dominated by CO_2 and H_2O[29]-[30]. The discrete ordinate (DO) model which can simulate the radiation transfer of both surface radiation and gaseous radiation [16][31], was adopted in this work. The emissivity ε of the chamber wall was assumed to be 0.8, as suggested by Agostinelli et al. [10], while the absorptivity α of the gaseous mixture was estimated by the weighted-sum-of-grey-gases (WSGG) approach.

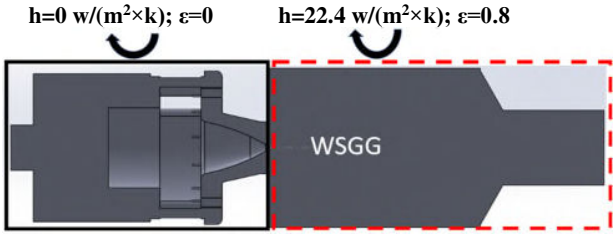

Figure 8. Low-pressure burner heat loss configuration

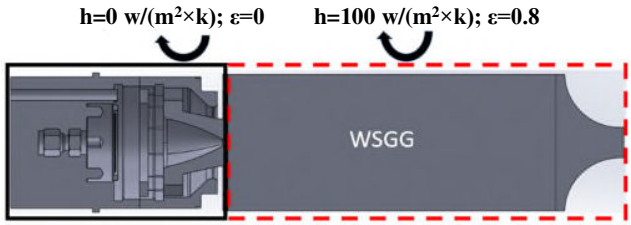

Figure 9. Higher pressure burner heat loss configuration

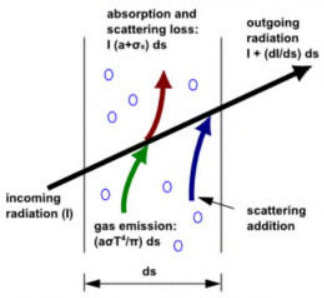

Figure 10. Gaseous radiative heat transfer [31]

The gaseous radiative heat transfer process is presented in **Figure 10**, and can be mathematically expressed as[31][32]:

$$\frac{dI(\vec{r},\ \vec{s})}{ds} + (\alpha + \sigma_s)I(\vec{r},\vec{s}) = \alpha n^2 \frac{\sigma T^4}{\pi} + \frac{\sigma_s}{4\pi}\int_0^{4\pi} I(\vec{r},\vec{s}')\Phi(\vec{s},\vec{s}')d\Omega' \quad (1)$$

Where $\vec{r}$ is the position vector, $\vec{s}$ is the direction vector, s is the path length (mean beam length), α is the gas mixture absorptivity, σ_s is scattering coefficient, n is the refractive index, σ is the Stefan-Boltzmann constant (5.67×10^{-8} $W\cdot m^{-2}\cdot K^{-4}$), $\vec{s}'$ is scattering direction vector, I is the radiation intensity (at the position vector $\vec{r}$ and direction $\vec{s}$), T is local temperature, Φ is phase function, Ω' is the solid angle.

Rajhi et al. [33] showed the scattering coefficient σ_s produced by CH_4, C_2H_6, C_3H_8 combustion was neglectable, because any soot particles produced were small, and the scattering intensity was a fourth-power function of soot particle diameter, thus the scattering effect was small and was neglected. In **Equation 1**, the α was estimated by weighted-sum-of-grey-gases (WSGG) method [29][34]. WSGG can use several grey

gases and a transparent gas to approach the emissivity of real non-grey gas, and the discrepancy between the grey gas and non-grey gas is corrected by applying some weighting factors [35]. Liu et al. [30], Xu et al. [34] and Shan et al. [35] show the WSGG is a good compromise to get accurate predictions with inexpensive computational consumption. Smith et al. [36] expressed the conventional WSGG model as:

$$\varepsilon = \sum_{i=0}^{I} a_{\varepsilon,i}(T)(1 - e^{-\alpha_i PS}) \quad (2)$$

$$\alpha = \sum_{i=0}^{I} a_{\alpha,i}(T, T_s)(1 - e^{-\alpha_i PS}) \quad (3)$$

Where T_S is the surface temperature, ε is the gas mixture emissivity, $a_{\varepsilon,i}$ is the emissivity weighting factor of i-th grey gas at gas temperature T. The $(1 - e^{-\alpha_i ps})$ denotes the emissivity of i-th grey gas, α_i is the absorption coefficient of i-th grey gas, PS is the partial pressure-path length. Also, P is the sum of the partial pressure of considered absorbing gases (carbon dioxide and water vapour), S is the beam length, $a_{\alpha,i}$ is the absorptivity weighting factor of i-th grey gas (as a function of gas temperature T and surface temperature T_s). Noticeably the species $i = 0$ is an assumed transparent gas with zero absorptivity coefficient (i.e., $\alpha_{i=0} = 0$) to meet the mathematical requirements (unity sum $\sum_{i=0}^{I} a_{\varepsilon,i}(T) = 1$ and $\sum_{i=0}^{I} a_{\alpha,i}(T, T_s) = 1$); so only the real radiative gas species starting from i=1 are included in the practical calculation[33]-[35].

3.3 Convection and Conduction Heat Loss Model

For the low pressure burner as presented in **Figure 8**, an external convection coefficient h=22.4W/(m^2·K) was calculated for the chamber wall using Refs [10][37]:

$$\overline{N_u} = 0.68 + \frac{0.67 Ra^{\frac{1}{4}}}{\left[1 + (0.492/Pr)^{\frac{9}{16}}\right]^{\frac{4}{9}}} \quad (4)$$

Where Ra is 5.8×10^6 and Pr is 0.7, as suggested by Agostinelli et al. [10] based on the LES study. To reduce CFD complexity, as shown in **Figure 8**, the burner center body was excluded from the low pressure burner model. As the upstream region (black rectangle of the figure) is "cool", the local convection coefficient h and emissivity ε are ignored (i.e., h=0 W/(m^2·K) and ε=0).

The heat loss of the higher pressure burner presented in **Figure 9** has an external cooling system (i.e., flow F in **Figure 4**) which does not enter the reaction zone. To model it, this work uses a convection coefficient h=100W/(m^2·K), suggested by Agostinelli et al. [10], to represent the cooling effect of flow F on the chamber's outer wall. Generally, the forced convection coefficient of air should be around h=10 to 500W/(m^2·K) [38], therefore this assumption of h=100W/(m^2·K) is reasonable.

As shown in **Figure 9**, the burner center body and bulkhead are included to model the heat conduction from the downstream reaction zone to the upstream burner region. Inside the solid bulkhead region, there is a cooling system (i.e., flow E in **Figure 4**) that would dominate the local heat loss. The upstream region (solid black rectangle in **Figure 9**) is "cool"; thus, the external natural convection h of the upstream region was neglected (i.e., assuming h=0W/(m^2·K) and ε=0).

3.4 Evaluation of NOx Emissions

Douglas et al. [1] and Breer et al. [26] show that it may be more appropriate to quote NOx emissions from CH_4/H_2 flames on a mass/energy basis. That is, emitted NOx mass per unit of fuel energy input $\dot{m}_{NO_X}/P_{th}$ rather than on a volume concentration basis in ppmv, corrected to 15% O_2, dry. This is because CH_4/H_2 flames produce more water vapour and consume less oxygen than a CH_4 flame. This means that the corrected ppmv basis could overestimate the change in NO_X concentration of CH_4/H_2 flames relative to a CH_4 flame for the same energy input. Also, for the same overall NOx emission (total moles or mass) due to the correction to "dry conditions and 15%O_2".

For the mass/energy approach, and keeping a constant energy input, Breer et al. [26] showed that the NO_X produced by CH_4/H_2 flames decreased as the H_2 was increased. This is possible because the prompt NOx was suppressed by the decrease in carbon atoms [3]. Noticeably, Breer's work was performed using a low-order (0-D or 1-D) chemical reactor model, which assumed the fuel and air were fully premixed and did not account for the impact of burner geometry, flame stretch and fuel/air mixing quality on the NOx emission. The present study uses both approaches to corroborate the observations from open literature.

4. EXPERIMENTAL METHOD

Experimental works were performed by Meier et al. [9] and Chterev and Boxx [11], which presents the velocity field measured by particle image velocimetry (PIV) technology. Also, the OH* signal measured by Chemiluminescence (OH*-CL) and Planar Laser-induced Fluorescence (OH*-PLIF) technologies to indicate the flame shape. This is in relation to the low pressure and higher pressure PRECCINSTA burner in **Sections 5** and **6,** respectively. For the low pressure burner, the operating conditions are provided in the experimental work of Meier et al. [9]. This is for pure CH_4 fueled at 1 bar and 30kW to measure the flame temperature and CO_2. The 27kW case was also considered, with measurements of the velocity field. **Table 1** presents the operating conditions of the referred work. For the higher pressure experimental PRECCINSTA burner, detailed operating conditions and OH*-CL results were provided by DLR. This is also available in Refs [11] for the 5 bar CH_4/H_2 operation that applies to
Table 2**.**

Table 1. Low pressure PRECCINSTA burner experimental operating conditions [9]

p_{comb} [bar]	T_{air} [K]	$\dot{m}_{air}$ [g/s]	$\dot{m}_{CH_4}$ [g/s]	T_{fuel} [K]	P_{th} [kW]	Φ
1.01	320	12.24	0.60	300	30	0.83
1.01	320	12.24	0.54	300	27	0.75

Table 2. Higher pressure PRECCINSTA burner experimental operating conditions [11]

H_2 in fuel [vol%]	p_{comb} [bar]	T_{air} [K]	$\dot{m}_{air}$ [g/s]	$\dot{m}_{CH_4}$ [g/s]	$\dot{m}_{H_2}$ [g/s]	T_{fuel} [K]	P_{th} [W]
0%	5.08	633	92.2	3.70	0.00	300	185
20%	5.06	637	91.1	3.44	0.11	300	185
40%	5.01	642	89.5	3.08	0.26	300	185

5. LOW-PRESSURE BURNER ANALYSIS WITH CH_4

This section presents the qualitative comparison between the CFD models (FGM & EDC) and the experimental work (in **Figure 12a**) that shows OH*-PLIF signals measured to indicate the flame location and heat release rate[9][10]. Noticeably, the CFD results show the estimated base-state OH concentration rather than the excited OH* radical. The * applies to experimental analysis that results from emitted light when a laser is used to excite OH molecules. **Figure 11** is the mass fraction for OH for the FGM and EDC, showing the different zones of a swirl-stabilized flame depicted in **Figure 5**. **Figures 11** and **12** show that FGM did not correctly capture the flame pattern, while EDC captured an "M-shape" OH pattern like the experimental OH*-PLIF result, and the flame was anchored at the ISL. In **Figure 12b**, EDC shows an overestimation of OH concentration close to the tip of the burner centre body when compared to Agostinelli et al. [10] LES result in **Figure 12a**. In addition, the EDC also overestimated the flame length, as marked by the dashed line in **Figure 12b**.

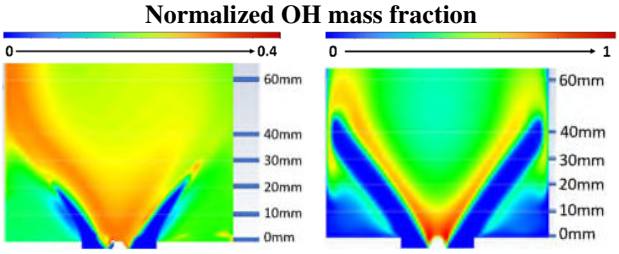

(a) FGM **(b) EDC**

Figure 11. Mass fraction of OH at 1bar 30kW

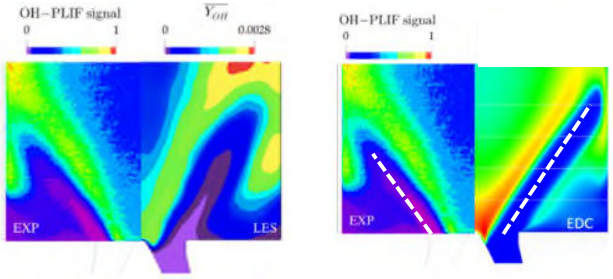

(a) EXP & LES [10] **(b) EXP & EDC**

Figure 12. Time-averaged OH*-PLIF signals and OH mass fraction at 1bar 30kW

Figure 13 is the velocity vector of the low pressure PRECCINSTA burner, showing a typical swirling flow pattern as depicted in **Figure 5**. **Figure 13** also shows that EDC was better at predicting the overall flame patterns than FGM, as the EDC better captured the symmetrical flow field close to the mixing tube exit. Several locations downstream of the mixing tube exit from 0mm to 60mm are marked in the figure.

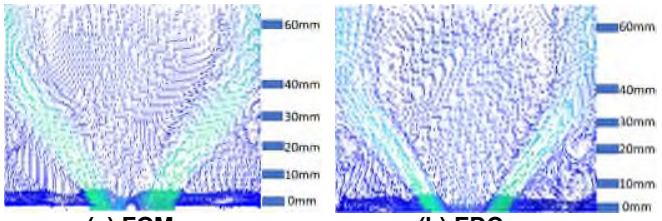

(a) FGM **(b) EDC**

Figure 13. Vector of velocity at 1bar 27kW

Figures 14 and **15** are the radial temperature profiles and CO_2 mass fraction profiles at different downstream locations. It shows that the ISL and OSL have high temperatures and high CO_2 mass fraction because the flame surface is stabilized at ISL and OSL. They also show that EDC has a better agreement with experimental results than FGM in estimating temperature and CO_2 mass fraction. But **Figure 14** shows that EDC underestimated the reaction rate and temperature of the fresh gas in-flow, as marked at h=30mm. The fresh gas in-flow was located between the ISL and the OSL, as depicted in **Figure 5**. Similarly, **Figure 15** shows that EDC underestimated the reaction rate of fresh gas in-flow, which resulted in a corresponding underestimation in CO_2 concentration, as marked at h=30mm. The underestimated reaction rate also resulted in an overestimation in flame length, as shown in **Figure 12b**. The local maximum differences and averaged overall differences between CFD results and experimental data were estimated and presented in **Table 3**. Note that the overall % error is an averaged value over each measured point along the radial distance.

Table 3. The error between CFD and experimental data for low pressure burner at 1bar 30kW and 27kW

	Temperature	*CO_2*	*axial velocity*
FGM maximum % error	61%	73%	asymmetric
FGM overall % error	30%	20%	20%
EDC maximum % error	27%	46%	33%
EDC overall % error	10%	5%	15%

Compared to EDC, the FGM showed a larger % error between predicted and measured flame temperature and CO_2 production, as shown in **Figure 14** and **Figure 15**. This is because FGM overestimated the fuel concentration in the inner recirculation zone (IRZ) and underestimated the fuel concentration in the outer recirculation zone (ORZ) when compared with experimental results. This resulted in a corresponding

overestimation of flame temperature in the IRZ and an underestimation in the ORZ shown in **Figures 14 and 16**. FGM also overestimated the reaction rate, as shown in **Figure 15**, where FGM predicted the combustion completed early at h=30mm. This comparison shows that EDC performed better at predicting temperature and CO_2 profiles than FGM.

Figure 17 presents the axial velocity U profiles at different downstream locations, showing that the fresh in-flow region produces peak positive axial velocity, while IRZ produces negative axial velocity due to recirculation flow. It also shows that EDC gave good agreement with experimental data in estimating the axial velocity U. The maximum difference between EDC and the experiment is seen at h=25mm and 35mm, where EDC underestimated the velocity in the fresh gas region between ISL and OSL. This is consistent with features seen previously in **Figure 14** which shows that EDC underestimates the temperature of the fresh gas region. Therefore, overestimates the fresh gas density with the constant mass flow. Hence, the fresh gas flow velocity U is consequently underestimated. Compared to EDC, the FGM did not correctly capture the symmetry of velocity profiles, especially from h=1.5mm to h=5mm. This comparison showed EDC had a better performance in predicting velocity profiles than FGM. Details of the radial velocity V are presented in **Appendix C**.

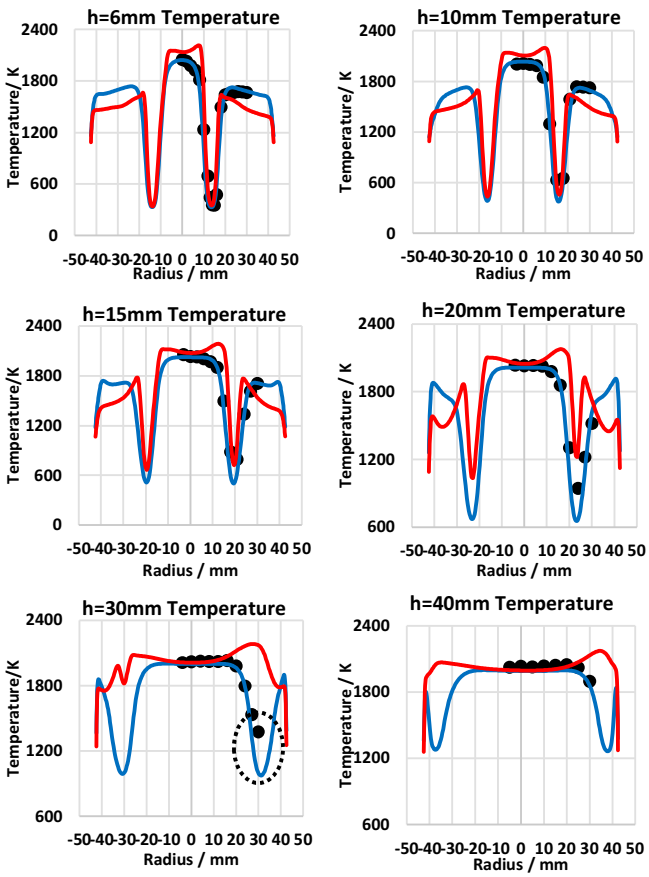

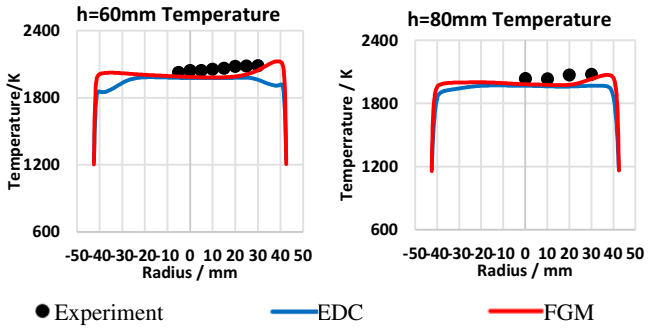

Figure 14. Temperature profiles at 1bar 30kW

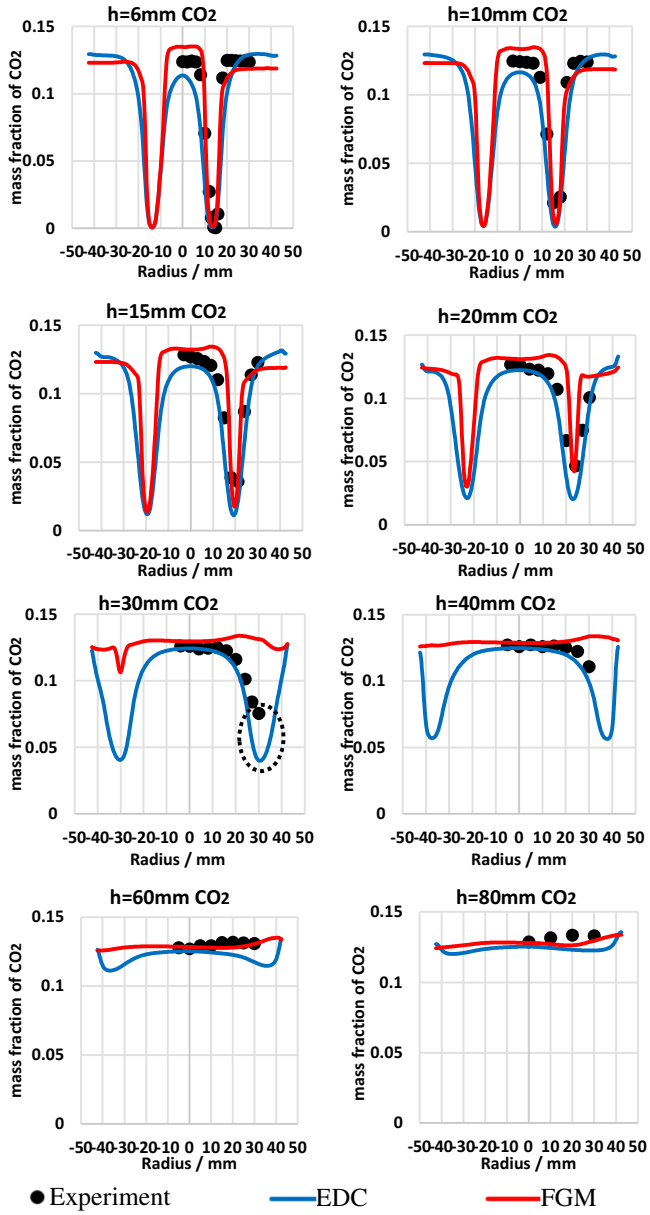

Figure 15. Mass fraction of CO_2 at 1bar 30kW

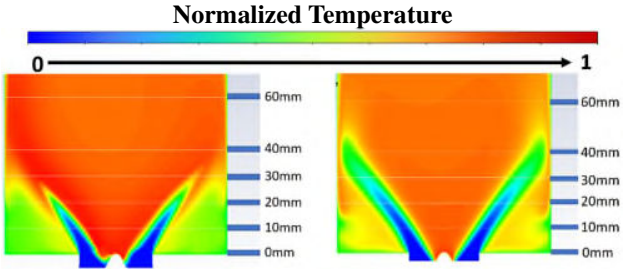

(a) FGM (b) EDC

Figure 16. Contour plot of temperature at 1bar 30kW

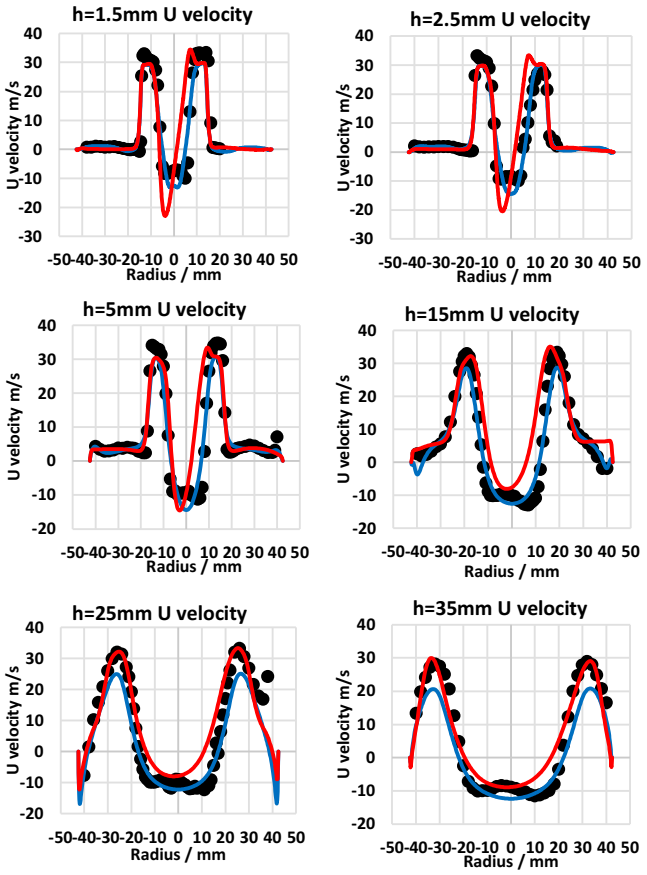

Figure 17. Axial velocity U profiles at 1bar 27kW

Figure 11 to **Figure 17** have shown that for this CH_4-fueled low pressure PRECCINSTA burner, EDC agrees more closely with the experimental results than FGM. The major swirl-stabilized flame pattern was captured by EDC with a much lower computation cost than LES. However, EDC underestimated the reaction rate of the fresh gas region between ISL and OSL. This resulted in a corresponding underestimation of flame temperature T, CO_2 mass fraction and flow velocity (inside the fresh gas region), especially at h=30mm, where the maximum difference was around 30% lower than experimental data.

6. HIGHER PRESSURE BURNER ANALYSIS WITH CH_4/H_2

This section focuses on the use of EDC to model CH_4/H_2 blends at 5 bar and check the predictions of the model against the experiments at the conditions shown in **Table 2**. **Figure 18** is the velocity vector and velocity magnitude at 5bar 40vol% H_2, showing that the flame is anchored at the ISL where the velocity magnitude is low enough to sustain an equilibrium between flow velocity and flame speed. **Figure 19** is the temperature contour of varied hydrogen contents, showing that the flame surface is very thin and stabilized at the ISL as well. It also shows that as the H_2 is increased, the chemical reaction rate increases and the flame length decreased. The tip of the flame surface decreased from 50 mm at 0vol%H_2 to 40mm at 20vol%H_2. There is a further decrease to 35mm at 40vol%H_2. This is consistent with the trend of the experimental results as shown in **Figure 20(b),** indicating that the EDC model adequately captures the flame length. Although H_2 varied from 0vol% to 40vol%, the flame temperature fields did not change significantly because the fuel energy input (185kW, evaluated by lower heating value) was kept constant.

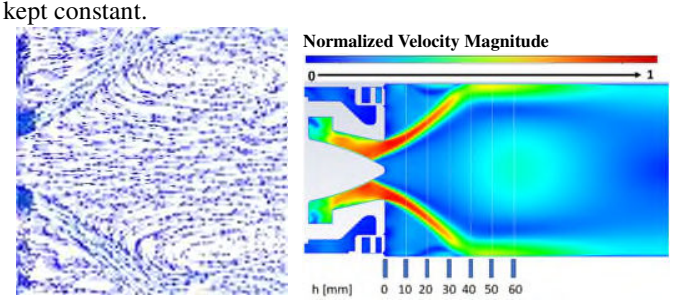

(a) Velocity vector (b) Velocity magnitude

Figure 18. Velocity characteristics at 40 vol%H_2

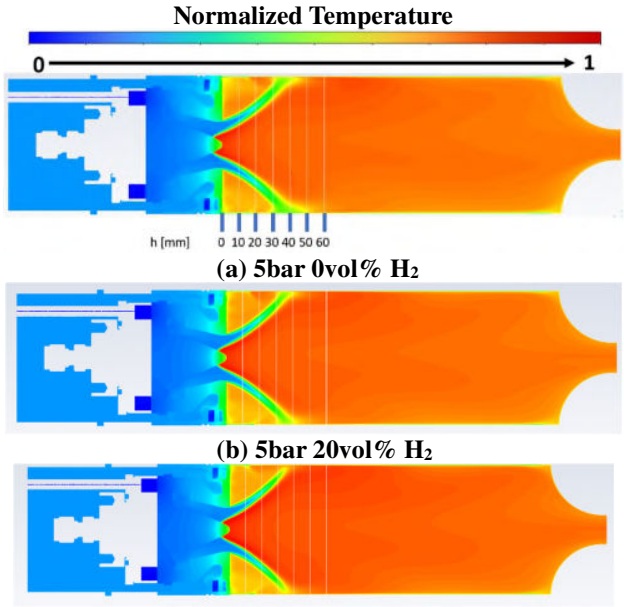

(a) 5bar 0vol% H_2

(b) 5bar 20vol% H_2

(c) 5bar 40vol% H_2

Figure 19. Contours of temperature at different CH_4/H_2 blends

Figure 20 presents OH signals that indicate the flame location and heat release rate. The figure shows that the EDC and experimental results are similar. They both show that the chemical reaction rate and the maximum OH intensity increased as the hydrogen was increased and caused a decrease in flame length. The maximum OH concentrations were seen at the ISL, indicating the flame was anchored at the ISL and the major reactions were completed in the ISL.

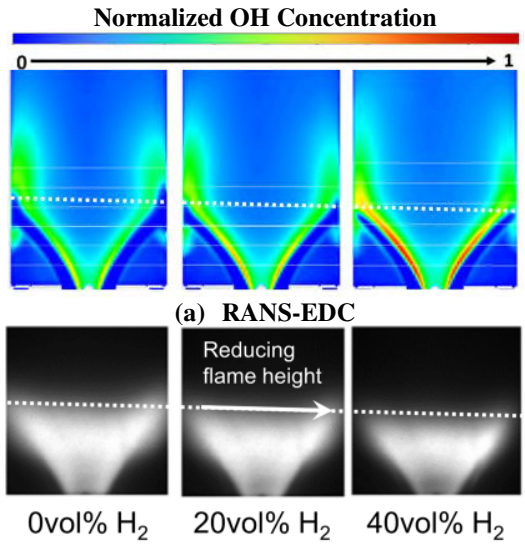

(a) RANS-EDC

(b) Experiment OH*-CL [11]

Figure 20. OH concentration for CH_4/H_2 blends

Table 4. Combustor exit characteristics – EDC model

H_2%vol in fuel	0vol%	20vol%	40vol%
Outlet temperature T_{out} [K]	1877	1886	1903
C_p at combustor outlet [J/(kg·K)]	1404	1412	1424
Mass fraction of NO_X at combustor outlet (Y_{NO_X})	1.80×10^{-4}	1.83×10^{-4}	1.72×10^{-4}
NO_X mass emits $\dot{m}_{NO_X}$ [g/s]	1.73×10^{-2}	1.73×10^{-2}	1.59×10^{-2}
NO_X mass emits per unit of energy input $\frac{\dot{m}_{NO_X}}{P_{th}}$ [ng/J]	93.3	93.6	86.3
corrected ppmvdr NO_X	86.4	88.4	83.3

By keeping the fuel energy input P_{th} (185kW) the same for all cases of blends, the combustor outlet temperature was expected to be approximately constant. However, **Table 4** shows a slight increase in outlet temperature T_{out}, due to the difference in air mass flow rate $\dot{m}_{air}$ and air inlet temperature T_{air} as presented in **Table 2**.

Figure 21 is the radial temperature profiles at different downstream locations, showing that ISL and OSL have high temperatures, as major reactions are completed at ISL and OSL. It also shows that as H_2 was increased, the local flame temperature at ISL increased; this is due to the enhanced reaction rate. The corresponding profiles of radial OH mass fraction are shown in **Figure 22.** It is observed here, from 10mm to 50mm, 40% H_2 exhibits a higher OH concentration than 0% and 20% at the ISL, indicating an enhanced reaction rate with higher hydrogen content. This trend is consistent with the temperature profiles shown in **Figure 21**. At 60mm, the 40% H_2 case presents a lower OH concentration than the 0% and 20% cases. This is because the major chemical reaction has been completed by 60mm, resulting in a decreased reaction rate and lower OH concentration. The asymmetry observed in the radial temperature and OH profiles is due to the rectangular shape of the chamber. However, this asymmetry for the temperature profile is minimally reduced when hydrogen is increased (at 50 and 60mm). This is because complete combustion is achieved at a shorter distance with higher hydrogen.

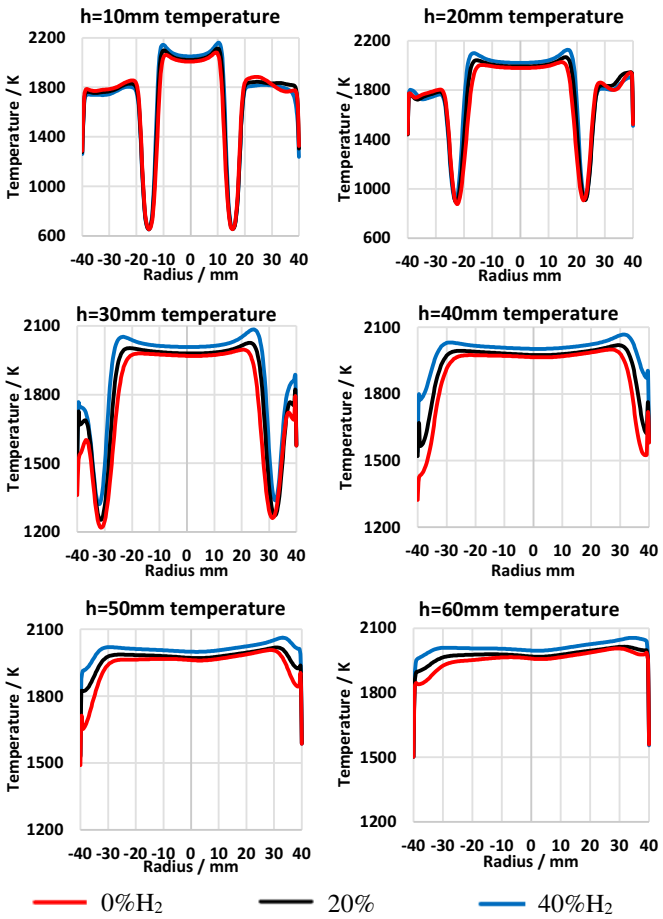

Figure 21. Temperature profiles at different downstream locations with different CH_4/H_2 blends

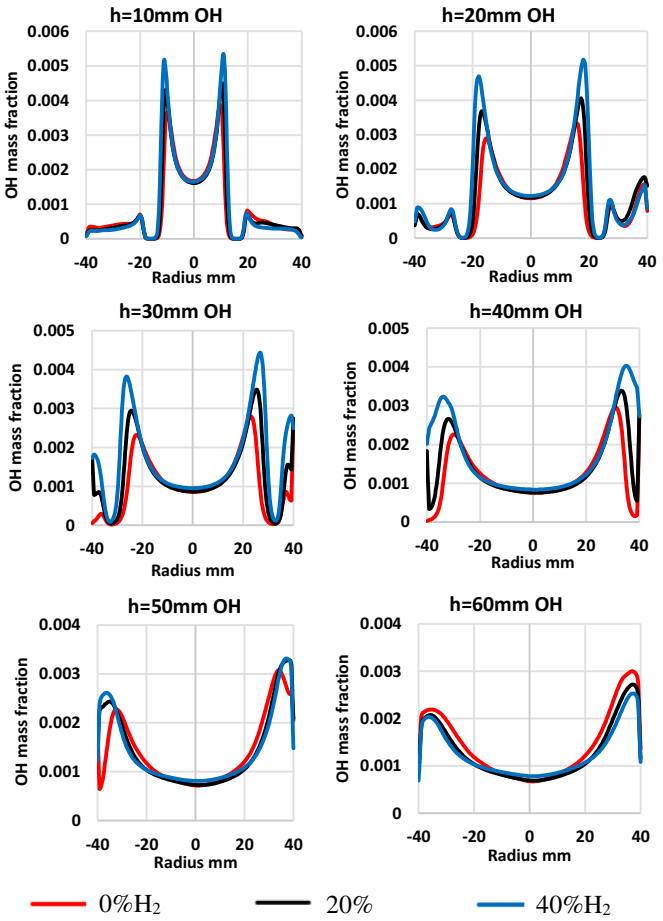

Figure 22. OH mass fraction at different downstream locations with different CH_4/H_2 blends

Figure 23 presents the axial velocity profiles at the downstream locations. It also shows that as the H_2 was increased, the reaction rate of the fresh gas region increased, the local temperature increased and resulted in a decrease in local density. As the mass flow was kept approximately constant, the velocity of the fresh gas region was enhanced. But this impact on the overall velocity field was not significant because the energy input was kept constant.

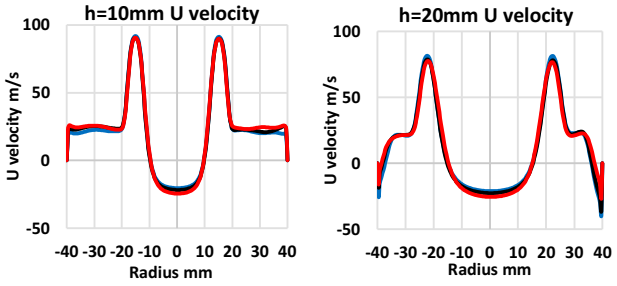

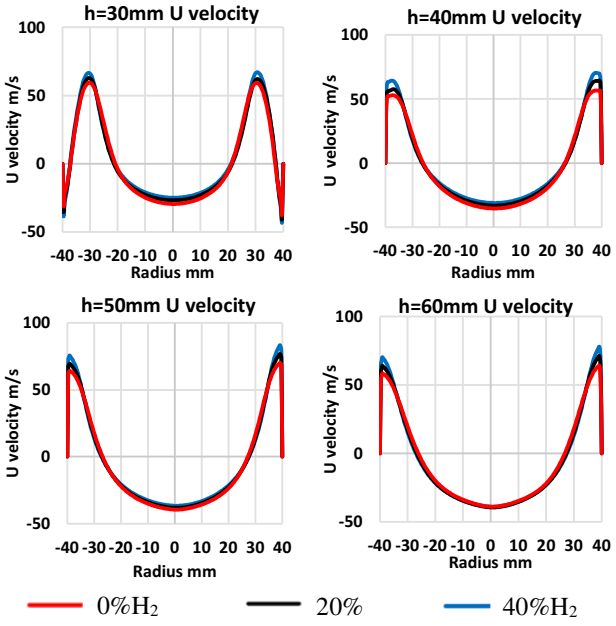

Figure 23. Axial velocity at different downstream locations with different CH_4/H_2 blends

As discussed in **Section 3.4**, it is appropriate to quote NO_X emission from CH_4/H_2 flames on a mass/energy basis (i.e., emitted NO_X mass per unit of fuel energy input $\dot{m}_{NO_X}/P_{th}$) rather than on a ppmv basis (corrected 15%O_2, dry). Detailed definitions of mass and ppmv-basis can be found in Breer et al[26] and Douglas et al[1]. This study adopts both methods and presents the outcomes in **Figure 24**. It should be noted that the NOx presented is the average concentration at the combustor outlet. For the mass basis shown in the figure, it indicates that as H_2 is increased from 0 to 20vol%, there was no significant change in NO_X emission, but from 20 to 40vol% NO_X it reduces. This is possibly due to the formation of prompt NO_x suppressed by the decrease in carbon atoms [3]. However, the decrease in NO_x due to the suppression of the formation of prompt NO_X is unlikely to be significant given the relatively modest H_2 content and the levels of NO_X emissions seen. Another reason is the mixing quality of fuel, and the air was improved as H_2 increased. This is shown in **Figure 25**, where the amount of fuel which was not fully premixed was evaluated by "unmixedness", and it decreased as the hydrogen was increased. As explained in Wiranegara et al. [39], a lower unmixedness value represents better mixing quality, which has a strong relationship with NO_x emissions. The mathematical definition of unmixedness used in the referred work was adopted in this paper. The influence of H_2 blending on "unmixedness" is because the momentum flux ratio of the fuel and air was impacted by the variance in fuel composition, which results in a change in fuel trajectory and fuel distribution (i.e., fuel/air mixing quality)[40].

As for the ppmv approach in **Figure 24**, it shows a similar trend as mass/energy results but predicted an increase in NOx emission from 0 to 20vol%, possibly because the ppmv approach tends to overestimate the NOx emission of hydrogen-contained

flame due to "15% O_2 and dry" corrections, as explained in **Section 3.4**. Thus, this work also recommends that absolute NOx emission is better represented by mass/energy basis.

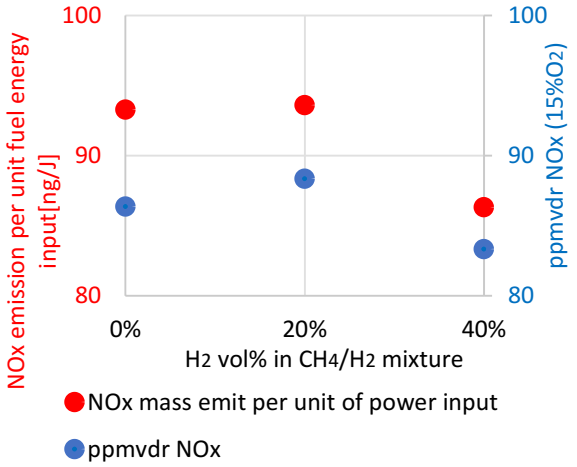

Figure 24. NO_X emissions for different blends of CH_4/H_2 using mass/energy and volume concentration – EDC model

Figure 26 shows the fuel distribution at the mixing tube exit with different CH_4/H_2 blends. It indicates little change in the overall fuel distribution (corrected equivalence ratio) with increasing H_2 content for the same fuel energy input. The consequence of a fixed energy input is that the global equivalence ratio decreases as H_2 concentration rises. It is important to mention that in the figure, the individual equivalence ratio at the mixing tube exit is divided by the global equivalence ratio before normalization for an appropriate comparison.

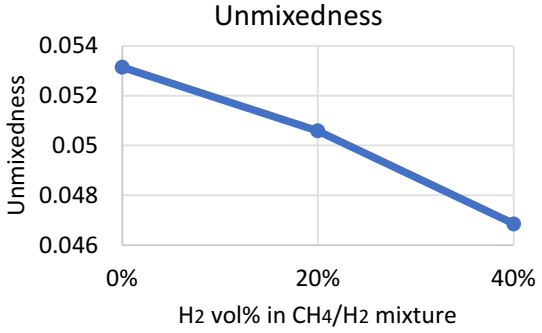

Figure 25. "Unmixedness" versus CH_4/H_2 blends

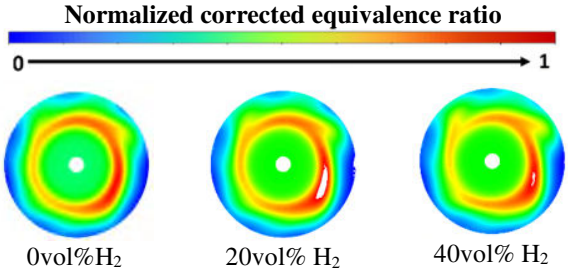

Figure 26. Corrected equivalence ratio at mixing tube exit

7. CONCLUSIONS

In summary, this study shows a RANS-CFD investigation into the modelling of hydrogen/methane blends in technically premixed flames. Good agreement with experimental data was achieved, justifying the approach. The work has demonstrated that:

- For the CH_4-fuelled low-pressure burner, the EDC model produced a significantly better agreement with experimental data than the FGM approach, justifying its additional computational time and cost.
- EDC generates a good representation of the main features of the flames produced by this burner and is suitable for use in a preliminary RANS study, however the tendency to underestimate the flame temperature in the fresh gas region and to overestimate flame length should be recognized.
- For the higher pressure study, the EDC model adequately captured the influence of H_2 addition in the combustion process for the blends of CH_4/H_2. This is characterised by the shortening in the flame length from 50mm at 0% case to 35mm at 40 vol%H_2. This is a key feature also observed from the experiment.
- At fixed fuel energy input P_{th} conditions, as the H_2 was increased, the predicted NOx (quoted on a mass/energy basis) decreased. Possible reasons for this are the suppression of the formation of prompt NOx by the decrease in carbon atoms and improved fuel/air mixing quality.

8. ACKNOWLEDGMENTS

The authors owe gratitude to German Aerospace Center (DLR). Institute of Combustion Technology. Particularly Dr Wolfgang Meier and Dr Isaac Boxx (now in Professor at RWTH Aachen University) for providing the CAD geometry and experimental data used. The ideas and opinions expressed here are those of the authors.

REFERENCES

[1] Douglas, C. M., Shaw, S. L., Martz, T. D., Steele, R. C., Noble, D. R., Emerson, B. L., and Lieuwen, T. C., 2022, "Pollutant Emissions Reporting and Performance Considerations For Hydrogen–Hydrocarbon Fuels in Gas Turbines," *Proceedings of ASME Turbo Expo*, Rotterdam, The Netherlands.

[2] Wind, T., Güthe, F., and Syed, K., 2014, "Co-Firing of Hydrogen and Natural Gases in Lean Premixed Conventional and Reheat Burners (Alstom GT26)," *Proceedings of the ASME Turbo Expo*, pp. 1–9.

[3] Ueda, A., Nisida, K., Matsumura, Y., Ichikawa, T., Nakashimada, Y., Endo, T., and Kim, W., 2021, "Effects of Hydrogen and Carbon Dioxide on the Laminar Burning Velocities of Methane–Air Mixtures," J. Energy Inst., **99**(June), pp. 178–185.

[4] Griffiths, A., and Syred, N., 2010, "Flashback Limits of Premixed H2/CH4 Flames in a Swirl-Stabilized Combustor," *Proceedings of ASME Turbo Expo*, Glasgow, UK, pp. 1–12.

[5] Ruan, S., Swaminathan, N., Isono, M., Saitoh, T., and Saitoh,

K., 2015, "Simulation of Premixed Combustion with Varying Equivalence Ratio in Gas Turbine Combustor," J. Propuls. Power, **31**(3), pp. 861–871.

[6] Zghal, M., Sun, X., Gauthier, P. Q., and Sethi, V., 2020, "Comparison of Tabulated and Complex Chemistry Turbulent-Chemistry Interaction Models with High Fidelity Large Eddy Simulations on Hydrogen Flames," *Proceedings of the ASME Turbo Expo*, pp. 1–11.

[7] Shrivastava, S., Verma, I., Yadav, R., Nakod, P., and Orsino, S., 2021, "Comparison of Performance of Flamelet Generated Manifold Model with That of Finite Rate Combustion Model for Hydrogen Blended Flames," *Proceedings of the ASME Turbo Expo*, pp. 1–13.

[8] Patil, S., Cooper, J., Orsino, S., Meadows, J., Valdes, R., and Laster, W. R., 2016, "Investigation of Single-Jet Combustor Near Lean Blowout Conditions Using Flamelet-Generated Manifold Combustion Model and Detailed Chemistry," J. Eng. Gas Turbines Power, **138**(12), pp. 1–7.

[9] Meier, W., Weigand, P., Duan, X. R., and Giezendanner-Thoben, R., 2007, "Detailed Characterization of the Dynamics of Thermoacoustic Pulsations in a Lean Premixed Swirl Flame," Combust. Flame, **150**(1–2), pp. 2–26.

[10] Agostinelli, P. W., Laera, D., Boxx, I., Gicquel, L., and Poinsot, T., 2021, "Impact of Wall Heat Transfer in Large Eddy Simulation of Flame Dynamics in a Swirled Combustion Chamber," Combust. Flame, **234**.

[11] Chterev, I., and Boxx, I., 2021, "Effect of Hydrogen Enrichment on the Dynamics of a Lean Technically Premixed Elevated Pressure Flame," Combust. Flame, **225**, pp. 149–159.

[12] Gong, Y., Fredrich, D., Marquis, A. J., Jones, W. P., and Boxx, I., 2021, "Thermoacoustic Instabilities of Hydrogen-Enriched Partially Premixed Flames in a Swirl Combustor," *Proceedings of the ASME Turbo Expo*, pp. 1–8.

[13] Wang, Z., 2017, "Interaction Between Precessing Vortex Core and Thermoacoustic Coupling in a Lab-Scale Lean Premixed Gas Turbine Combustor: Numerical Simulation Studies," *Proceedings of ASME Turbo Expo*, pp. 1–9.

[14] Combustion, B., Simulation, N., The, O. F., Burner, P., On, B., and Sound, S., 2016, "Broadband Combustion Noise Simulation of the PRECCINSTA Burner Based on Stochastic Sound Sources," *Proceedings of ASME Turbo Expo*, pp. 1–13.

[15] Slabaugh, C. D., Boxx, I., Werner, S., Lucht, R. P., and Meier, W., 2016, "Structure and Dynamics of Premixed Swirl Flames at Elevated Power Density," AIAA J., **54**(3), pp. 946–961.

[16] ANSYS Inc., 2021, *FLUENT User's Guide 21 R1*.

[17] Ottino, G. M., Fancello, A., Falcone, M., Bastiaans, R. J. M., and De Goey, L. P. H., 2016, "Combustion Modeling Including Heat Loss Using Flamelet Generated Manifolds: A Validation Study in OpenFOAM," Flow, Turbul. Combust., **96**(3), pp. 773–800.

[18] Langone, L., Amerighi, M., and Andreini, A., 2022, "Large Eddy Simulations of a Low-Swirl Gaseous Partially Premixed Lifted Flame in Presence of Wall Heat Losses†," Energies, **15**(3).

[19] Sun, X., Agarwal, P., Carbonara, F., Abbott, D., Gauthier, P., and Sethi, B., 2020, "Numerical Investigation into the Impact of Injector Geometrical Design Parameters on Hydrogen Micromix Combustion Characteristics," *Proceedings of the ASME Turbo Expo*, pp. 1–11.

[20] Jin, U., and Kim, K. T., 2021, "Experimental Investigation of Combustion Dynamics and NOx/CO Emissions from Densely Distributed Lean-Premixed Multinozzle CH4/C3H8/H2/Air Flames," Combust. Flame, **229**(x), p. 111410.

[21] He, G., Guo, Y., Hsu, A. T., Brankovic, A., Syed, S., and Liu, N. S., 1999, "The Effect of Schmidt Number on Turbulent Scalar Mixing in a Jet-in-Crossflow," *Proceedings of the ASME Turbo Expo*.

[22] Li, S., Zhang, S., Hou, L., and Ren, Z., 2018, "Analysis of the Mixing and Emission Characteristics in a Model Combustor," *Proceedings of the ASME Turbo Expo*, pp. 1–7.

[23] Nanduri, J. R., Parsons, D. R., Yilmaz, S. L., Celik, I. B., and Strakey, P. A., 2010, "Assessment of RANS-Based Turbulent Combustion Models for Prediction of Emissions from Lean Premixed Combustion of Methane," Combust. Sci. Technol., **182**(7), pp. 794–821.

[24] Jella, S., Gauthier, P., Bourque, G., Bergthorson, J., Bulat, G., Rogerson, J., and Sadasivuni, S., 2018, "Large Eddy Simulation of a Pressurized, Partially Premixed Swirling Flame with Finite-Rate Chemistry," J. Eng. Gas Turbines Power, **140**(11), pp. 1–9.

[25] "GRI-Mech 3.0" [Online]. Available: http://combustion.berkeley.edu/gri-mech. [Accessed: 19-Nov-2021].

[26] Breer, B., Rajagopalan, H. P., Godbold, C., Ii, J., Emerson, B., Acharya, V., Sun, W., Lieuwen, T., and Noble, D., 2022, "NOx Production from Hydrogen-Methane Blends," *In Spring Technical Meeting of the Eastern States Section of the Combustion Institute, Orlando, FL, Mar. 6-9*, pp. 149RKF–0019.

[27] Donohoe, N., Heufer, A., Metcalfe, W. K., Curran, H. J., Davis, M. L., Mathieu, O., Plichta, D., Morones, A., Petersen, E. L., and Güthe, F., 2014, "Ignition Delay Times, Laminar Flame Speeds, and Mechanism Validation for Natural Gas/Hydrogen Blends at Elevated Pressures," Combust. Flame, **161**(6), pp. 1432–1443.

[28] Santner, J., Ahmed, S. F., Farouk, T., and Dryer, F. L., 2016, "Computational Study of NOx Formation at Conditions Relevant to Gas Turbine Operation: Part 1," Energy and Fuels, **30**(8), pp. 6745–6755.

[29] Jiang, L. Y., and Campbell, I., 2009, "Radiation Benchmarking in a Model Combustor," J. Eng. Gas Turbines Power, **131**(1).

[30] Liu, F., Becker, H. A., and Bindar, Y., 1998, "A Comparative Study of Radiative Heat Transfer Modelling in Gas-Fired Furnaces Using the Simple Grey Gas and the Weightedsum-of-Grey-Gases Models," Int. J. Heat Mass Transf., **41**(22), pp. 3357–3371.

[31] ANSYS Inc., 2021, *Ansys Fluent Theory Guide 21 R1*.

[32] Raghib Shakeel, M., Sanusi, Y. S., and Mokheimer, E. M. A., 2017, "Numerical Modeling of Oxy-Fuel Combustion in a Model Gas Turbine Combustor: Effect of Combustion Chemistry and Radiation Model," Energy Procedia, **142**, pp. 1647–1652.

[33] Rajhi, M. A., Ben-Mansour, R., Habib, M. A., Nemitallah, M. A., and Andersson, K., 2014, "Evaluation of Gas Radiation Models in CFD Modeling of Oxy-Combustion," Energy Convers. Manag., **81**, pp. 83–97.

[34] Xu, J., Chen, R., and Meng, H., 2021, "WSGG Models for Radiative Heat Transfer Calculations in Hydrogen and Hydrogen-Mixture Flames at Various Pressures," Int. J. Hydrogen Energy, **46**(61), pp. 31452–31466.

[35] Shan, S., Qian, B., Zhou, Z., Wang, Z., and Cen, K., 2018, "New Pressurized WSGG Model and the Effect of Pressure on the Radiation Heat Transfer of H2O/CO2 Gas Mixtures," Int. J. Heat Mass Transf., **121**, pp. 999–1010.

[36] Smith, T. F., and Shen, Z. F., 1981, "Evaluation of Coefficients for the Weighted Sum of Gray Gases Model.," Am. Soc. Mech. Eng., **104**(November).

[37] Churchill, S. W., and Chu, H. H. S., 1975, "Correlating Equations for Laminar and Turbulent Free Convection From a Vertical Plate," Inr. J. Heal Moss Transf., **18**, pp. 1323–1329.

[38] Kosky, P., Balmer, R., Keat, W., and Wise, G., 2020, *Exploring Engineering: An Introduction to Engineering and Design, Fifth Edition*, Elsevier.

[39] Wiranegara, R. Y., Igie, U., Ghali, P., Zhao, R., Abbott, D., and Hamilton, R., 2022, "Numerical Study of Radiation and Fuel – Air Unmixedness on the Performance of a Dry Low NOx Combustor," ASME Open J. Eng., **1**, pp. 1–13.

[40] Holdeman, J. D., 1972, "Correlation for Temperature Profiles in the Plane of Symmetry Downstream of a Jet Injected Normal to a Crossflow," NASA Tech. Note NASA TN D-6966, (September).

Appendix A. Grid independence study

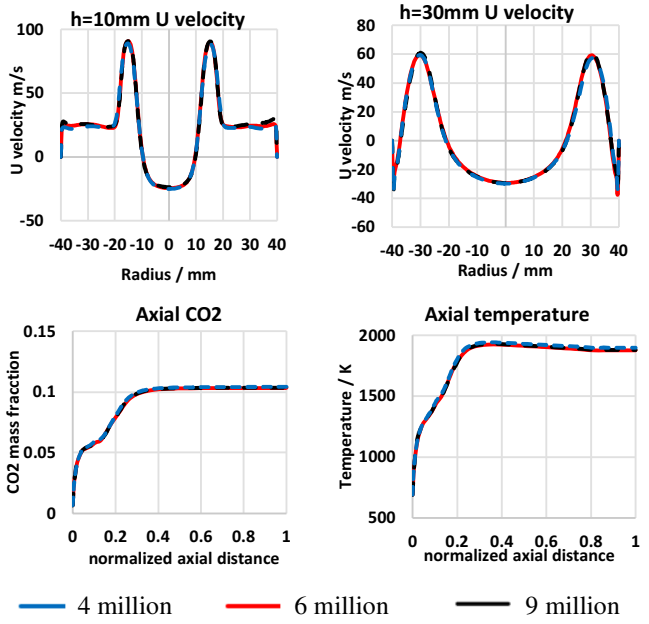

Figure A1. Grid independence study on velocity, CO_2 mass fraction temperature in the axial plane

Appendix B. Comparison of turbulence models with experimental data

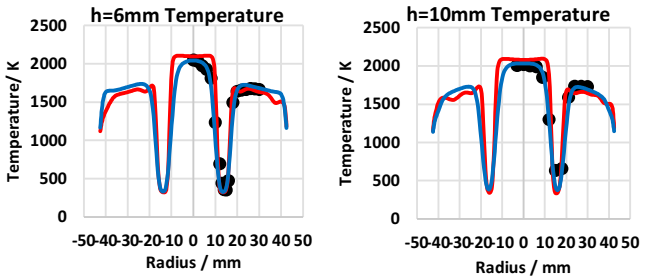

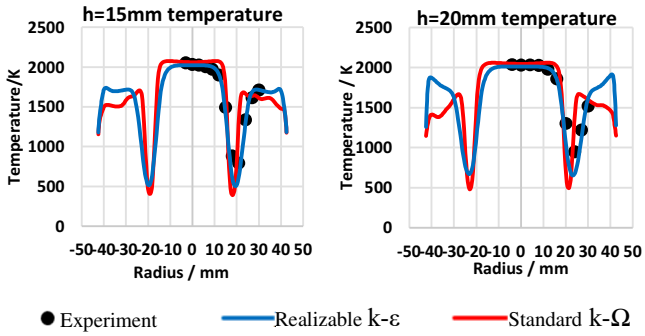

Figure B1. Temperature profiles of low pressure burner for turbulence models and experimental data at 1bar 30kW using EDC

Appendix C. Low pressure burner radial velocity at 1bar 27kW

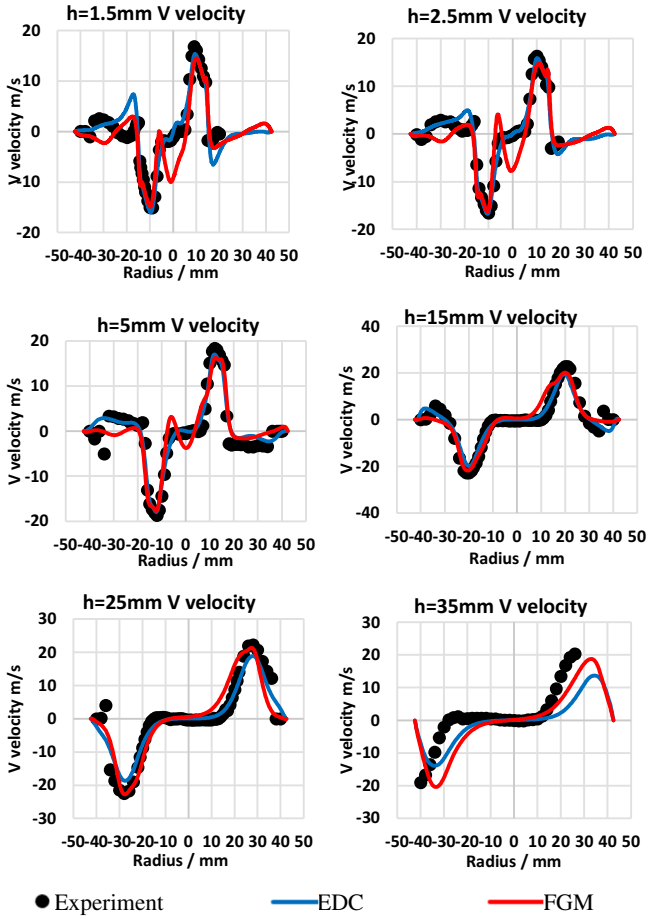

Figure C1. Low pressure burner radial velocity V at 1bar 27kW for CFD models and experiment

2023-09-28

Hydrogen-enriched natural gas co-firing: a comparison of FGM and EDC models

Zhao, Rang

American Society of Mechanical Engineers

Zhao R, Igie U, Abbott D. (2023) Hydrogen-enriched natural gas co-firing: a comparison of FGM and EDC models. In: ASME Turbo Expo 2023: Turbomachinery Technical Conference and Exposition, 26-30 June 2023, Boston, USA. Paper number GT2023-103205

https://doi.org/10.1115/GT2023-103205